energies

MDPI

Article

Enhancement Effect of Bimetallic Amide $K_2Mn(NH_2)_4$ and In-Situ Formed KH and Mn_4N on the Dehydrogenation/Hydrogenation Properties of Li–Mg–N–H System

Gökhan Gizer [1], Hujun Cao [1,2], Julián Puszkiel [1,3,*], Claudio Pistidda [1], Antonio Santoru [1], Weijin Zhang [2], Teng He [2], Ping Chen [2], Thomas Klassen [1,4] and Martin Dornheim [1,*]

1 Nanotechnology Department, Helmholtz-Zentrum Geesthacht, Max-Planck Straße 1, 21502 Geesthacht, Germany
2 Dalian National Laboratory for Clean Energy Dalian Institute of Chemical Physics, Chinese Academy of Sciences, Dalian 116023, China
3 Consejo Nacional de Investigaciones Científicas y Técnicas (CONICET), Centro Atómico Bariloche, Av. Bustillo km 9500, S.C. de Bariloche, Argentina
4 Institut für Werkstofftechnik, Helmut-Schmidt-Universität, Holstenhofweg 85, 22043 Hamburg, Germany
* Correspondence: julian.puszkiel@hzg.de (J.P.); martin.dornheim@hzg.de (M.D.)

Received: 15 June 2019; Accepted: 15 July 2019; Published: 19 July 2019

Abstract: In this work, we investigated the influence of the $K_2Mn(NH_2)_4$ additive on the hydrogen sorption properties of the $Mg(NH_2)_2$ + 2LiH (Li–Mg–N–H) system. The addition of 5 mol% of $K_2Mn(NH_2)_4$ to the Li–Mg–N–H system leads to a decrease of the dehydrogenation peak temperature from 200 °C to 172 °C compared to the pristine sample. This sample exhibits a constant hydrogen storage capacity of 4.2 wt.% over 25 dehydrogenation/rehydrogenation cycles. Besides that, the in-situ synchrotron powder X-ray diffraction analysis performed on the as prepared $Mg(NH_2)_2$ + 2LiH containing $K_2Mn(NH_2)_4$ indicates the presence of Mn_4N. However, no crystalline K-containing phases were detected. Upon dehydrogenation, the formation of KH is observed. The presence of KH and Mn_4N positively influences the hydrogen sorption properties of this system, especially at the later stage of rehydrogenation. Under the applied conditions, hydrogenation of the last 1 wt.% takes place in only 2 min. This feature is preserved in the following three cycles.

Keywords: Bimetallic amide; hydrogen storage; amide-hydride; in situ X-ray diffraction; activation energy; reaction rate

1. Introduction

The use of renewable energy sources for fulfilling the world energy demand is one of the greatest challenges humankind has to face in the near future. Due to the intermittent nature and uneven distribution of these energy sources, an efficient energy vector must be found. In terms of energy storage, hydrogen is considered as a suitable candidate to solve this problem due to its high energy density (142 MJ/kg) (e.g. petroleum 47 MJ/kg) [1]. However, the conversion from a fossil fuel-based economy to a hydrogen-based economy is challenging. One of the key issues is the lack of an effective method to store hydrogen for stationary and mobile applications [2]. In the last decades, the possibility to store hydrogen in a solid state using metal hydride-based systems was investigated [3,4]. In this regard, several light metal complex hydrides such as alanates, borohydrides and amide-hydride systems were studied [5–11]. In particular, the reactive hydride composite (RHC) systems based on amide-hydrides are considered as promising hydrogen storage media, due to their suitable hydrogen

contents, good reversibility and tunable thermodynamic properties [9,12,13]. The first example of this class of material was the lithium imide/amide system according to reaction 1 [9].

$$Li_2NH + H_2 \leftrightharpoons LiNH_2 + LiH \qquad \Delta H = -45 \text{ kJ mol}^{-1} \tag{1}$$

After the publication of this pioneering work, several other amide-based RHC systems were synthesized and investigated [14]. Among them, the Li–Mg–N–H system attracted increasing attention due to its high hydrogen storage capacity (5.6 wt.%), favorable dehydrogenation enthalpy (ΔH: 40 kJ/mol-H_2) and good reversibility [15,16]. Theoretical calculations show that the thermodynamic properties allow for a rather low dehydrogenation reaction at 90 °C and a pressure of 1 bar of H_2, which is close to the operating temperature of proton exchange membrane fuel cells (PEMFCs) [17]. However, sufficient operating dehydrogenation rates have been obtained only at temperatures higher than 220 °C so far, due to kinetic constrains [18]. Several additives were used in order to improve the reaction properties of this system [19–29]. The introduction of KH leads to a sensible reduction of the dehydrogenation temperature attributed to the formation of $K_2Mg(NH_2)_4$ and $KLi_3(NH_2)_4$ during dehydrogenation [27]. These K-containing intermediates enable an energetically more favorable reaction pathway. The hydrogenation process of dehydrogenated $Mg(NH_2)_2$ + 2LiH appears to be more constrained than the first dehydrogenation [30,31]. In this regard, the addition of KH significantly improves the hydrogenation behavior [32]. Also RbH appears to be an excellent additive for enhancing the hydrogen sorption properties of this system [33,34]. Recently, the bimetallic amide-hydride systems $K_2Mn(NH_2)_4$ + 8LiH and $K_2Zn(NH_2)_4$ + 8LiH with ultrafast hydrogenation properties were reported by Cao et al. [35–37]. In these works, extremely fast hydrogenation of as much as 60% of the total H_2 capacity (1.75 wt.%) within 60 seconds was observed. These values are the fastest rehydrogenation rates in amide-hydride systems reported to date. The use bimetallic amides as additives on amide-hydride systems has not been investigated so far.

In this work, we studied the reaction properties of the $Mg(NH_2)_2$–2LiH–$x K_2Mn(NH_2)_4$ (x: 0–0.35) system. The effects of the addition of bimetallic amide $K_2Mn(NH_2)_4$ were investigated by means of calorimetric techniques, such as high pressure differential scanning calorimetry (HP-DSC) and differential thermal analysis (DTA) coupled with a mass spectrometer (MS). The material H_2 capacity was determined by volumetric technique (Sieverts apparatus), whereas the structural characterizations were performed via in-situ synchrotron powder X-ray diffraction (SR-PXD) method. This study provides new insight into the use of bimetallic amides as an additive on amide–hydride systems.

2. Materials and Methods

Starting materials for the synthesis of $K_2Mn(NH_2)_4$ are potassium (cubes, Sigma Aldrich, 99.5% purity, in mineral oil) and manganese (powder, Sigma Aldrich, ≥99% purity). A piece from the potassium cube was stirred with hexane in a jar several times to remove the mineral oil. $K_2Mn(NH_2)_4$ was synthesized by ball milling metallic potassium and manganese powders in a molar ratio of 2:1 with a ball to powder ratio 10:1 for 12 h with a speed of 100 rpm under an atmosphere of 7 bar of NH_3. PXD pattern of the post-milled sample confirmed the formation of the monoclinic $K_2Mn(NH_2)_4$ phase (Figure S1). Additionally, a tiny amount of (5 wt.%) cubic $MnH_{0.07}$ was formed. All milling procedures in this work were carried out in a Fritsch P6 ball miller, using a stainless steel milling vial (250 ml) and milling balls. The material handling and milling was carried out in a dedicated glove box under a continuously purified argon flow (O_2 and H_2O levels lower than 1 ppm).

$Mg(NH_2)_2$ was synthesized in house via a two-step process. Firstly, MgH_2 was ball milled at 400 rpm, under 7 bar of NH_3 pressure for 24 h. The vial was evacuated each 6 hours and refilled with fresh NH_3. In order to increase the material conversion yield, after ball milling, the material was heated to 300 °C under 7 bar of NH_3 for 24 hours in a high-pressure stainless steel reactor (20 ml) from the Parr Instrument Company. The purity of the obtained $Mg(NH_2)_2$ was above 95%, which was determined with thermogravimetric analysis (TG). Later, $Mg(NH_2)_2$ was ball milled with LiH and $K_2Mn(NH_2)_4$ (total amount: 1 g) for 36 h with a ball to powder ratio of 60:1 at 400 rpm under a pressure of 50 bar of

H_2. Three material batches with increasing quantities of $K_2Mn(NH_2)_4$ (i.e., 0.01, 0.05 and 0.35 mol) and four additional batches (one without additive and three batches containing KH additive) were prepared for comparison purposes. Sample compositions and designations are listed in Table 1.

Table 1. Compositions and designations for the investigated samples.

Sample Composition	Sample Code
$Mg(NH_2)_2$ + 2LiH	Mg–Li
$Mg(NH_2)_2$ + 2LiH + 0.01$K_2Mn(NH_2)_4$	Mg–Li–1KMN
$Mg(NH_2)_2$ + 2LiH + 0.05$K_2Mn(NH_2)_4$	Mg–Li–5KMN
$Mg(NH_2)_2$ + 2LiH + 0.35$K_2Mn(NH_2)_4$	Mg–Li–35KMN
$Mg(NH_2)_2$ + 2LiH + 0.07KH	Mg–Li–7KH
$Mg(NH_2)_2$ + 2LiH + 0.15KH	Mg–Li–15KH
$Mg(NH_2)_2$ + 2LiH + 0.30KH	Mg–Li–30KH

Volumetric differential pressure method was used for the determination of hydrogen storage properties of the as-milled and cycled composites. A homemade Sieverts apparatus was utilized for this purpose. About 100 mg of the sample was loaded into the sample holder in an Ar-filled glovebox (O_2 and H_2O levels lower than 1 ppm). All dehydrogenation/rehydrogenation measurements were performed under 1 bar of H_2 and under 80 bar of H_2, respectively, with a temperature ramp starting from room temperature (RT) to 180 °C. Details about the heating rate for each experiment were recorded in figure captions.

Multiple dehydrogenation/rehydrogenation cycles (25 cycle) of Mg–Li and Mg–Li–5KMN samples were performed in a high-pressure stainless steel autoclave from Estanit GmbH. The stainless steel specimen holder, which has six inlets, enables to simultaneously cycle several specimens under equal experimental conditions. However, due to the presence of specimens with different compositions, it is not possible to determine the gravimetric hydrogen capacities of each specimen. Powders of M–Li and Mg–Li–5KMN specimens were placed inside these inlets (~400 mg each) inside and Ar-filled glovebox (O_2 and H_2O levels lower than 1 ppm). Dehydrogenation/rehydrogenation were carried out under isothermal conditions at 180 °C, with pressures of 1 bar (dehydrogenation time: 20 hours) and 80 bar of H_2 (rehydrogenation time: 4 hours), respectively.

DTA/MS characterization of the materials was performed using Netzsch Simultaneous Thermal Analysis (STA) 409 and Hiden Analytical HAL 201 instruments, respectively. For performing these measurements, 10 mg of powder was loaded into an Al_2O_3 crucible and later placed into the DTA instrument, which is inside an Ar-filled glovebox (O_2 and H_2O levels lower than 1 ppm). Samples were heated from RT to 300 °C with a heating rate of 3 °C/min under 50 mL/min argon flow. The compositions of the gasses evolved during the DTA measurements were analyzed via MS technique.

SR-PXD experiments were performed at MAX II Synchrotron facility in Lund, Sweden, beamline I711 [38]. The instrumental geometry of the powder diffractometer is Debye–Scherrer. The used X-ray wavelength was λ = 0.9941 Å. The diffraction images were collected using an Agilent Titan detector (2048 × 2048 pixel, each of size 60 × 60 mm^2) placed at about 80 mm from the sample holder. The exact sample to detector distance and the instrumental function were obtained performing the Rietveld refinement (using the MAUD program) of the diffraction pattern of a LaB_6 standard specimen [39,40]. The powder was introduced into a sapphire capillary inside an Ar-filled glove box (O_2 and H_2O levels lower than 10 ppm) and then fixed into an in-house developed in-situ cell [41] which allows controlling the heating temperatures and operating gas pressures [42]. The first dehydrogenations were recorded in the temperature range between RT and 180 °C, with a heating rate of 5 °C/min under 1 bar of H_2. Following this experiment, the rehydrogenation process was recorded heating the material from RT to 180 °C under 80 bar of H_2 (heating ramp of 5 °C/min). The 2D images were integrated using the FIT2D software, and quantitative analysis were performed via the Rietveld method using the MAUD software [39,40,43].

The Effect of the additive addition on the kinetic behaviour of solid–gas reactions was evaluated also via the Kissinger method [44]. In fact, this method is suitable for the samples that exhibit multi-step reactions and it allows to determine the E_a of a reaction process without assuming a kinetic model. The equation for the E_a calculation is shown in Equation (1);

$$ln\left(\beta/T_m^2\right) = ln(AR/E_a) - \frac{E_a}{RT_m}, \quad (2)$$

where A is the pre-exponential factor and R is the gas constant. The temperature for the maximum reaction rate (T_m) was obtained from DSC curves measured at heating rates (β) of 1 °C/min, 3 °C/min, 5 °C/min and 10 °C/min under 1 bar of H_2 backpressure Then, $ln\left(\frac{\beta}{T_m^2}\right)$ against 1/T_m was plotted, and E_a and A was calculated from linear fitting.

3. Results and Discussion

3.1. First Dehydrogenation/Hydrogenation Properties

DTA curves and associated MS traces measured for the additive-free sample Mg–Li as well as the $K_2Mn(NH_2)_4$-containing samples (Table 1) are shown in Figure 1A–C. The Mg–Li sample exhibits an endothermic peak at 200 °C with a shoulder at 190 °C, which is in agreement with the two-step dehydrogenation pathway of $Mg(NH_2)_2$ + 2LiH [45]. At this temperature, mainly H_2 is released together with a small amount of NH_3. Above 225 °C, the release of NH_3 becomes dominant. Compared to the pristine system, the dehydrogenation reaction of the system containing 1 mol% $K_2Mn(NH_2)_4$ starts at a lower temperature (i.e., 110 °C), whereas the maximum of the dehydrogenation peak at 200 °C remains unchanged. When the additive amount is increased to 5 mol% (Mg–Li–5KMN), both dehydrogenation onset and peak temperature decrease to 80 °C and 172 °C, respectively. For both samples, Mg–Li–1KMN and Mg–Li–5KMN, the release of NH_3 below 200 °C is below the detection limit. However, increasing the amount of additives beyond 5 mol% (Mg–Li–35KMN) leads to significant NH_3 release, which starts at around 175 °C. Despite the fact that the dehydrogenation peak temperature of Mg–Li–35KMN is the lowest (143 °C), the H_2 peak area is also notably smaller in respect to those of the other samples. This is clearly due to the high amount of additive contained in this sample (~49 wt.%). Due to the pour amount of released H_2 and high amount of released NH_3, the sample Mg–Li–35KMN was not further investigated. DTA and MS results indicate that Mg–Li–5KMN has the optimum properties (among the investigated systems), since it presents the lowest H_2 release onset temperature (80 °C) with no NH_3 release until 200 °C.

In order to understand the reaction pathway of Mg–Li–5KMN, its dehydrogenation/rehydrogenation reactions were investigated via in-situ SR-PXD technique. The results of this investigation (PXD patterns as the function of temperature) are presented in the two-dimensional contour plot of Figure 2. The diffraction pattern acquired at RT (after ball milling) shows the existence of tetragonal $Mg(NH_2)_2$, cubic LiH, MgO and Mn_4N. Besides that, no $K_2Mn(NH_2)_4$ reflections are present. During the first dehydrogenation (Figure 2A), the reflections of cubic KH appear at 85 °C. At the same temperature, peaks belonging to orthorhombic $Li_2Mg(NH)_2$ are also observed. As the temperature increases, the intensity of the $Mg(NH_2)_2$ peaks diminishes and the intensity of the $Li_2Mg(NH)_2$ peaks increases. The continuous shift of the diffraction peaks towards lower 2θ angles, observed upon heating, is due to thermal expansion. Through the first hydrogenation attempt (Figure 2B), $Li_2Mg(NH)_2$ peak intensities start to decrease at 110 °C and a broad peak of $Mg(NH_2)_2$ appears at about 2θ = 9°. $Mg(NH_2)_2$ and LiH suddenly recrystallize at 165 °C (sharp $Mg(NH_2)_2$ and LiH peaks appear). The absence of peaks ascribable to $K_2Mn(NH_2)_4$ through all the first cycles indicates that during ball milling, $K_2Mn(NH_2)_4$ transforms into Mn_4N and a potassium compound with amorphous or nanocrystalline features. Therefore, $K_2Mn(NH_2)_4$ must be considered as a precursor for the formation of Mn_4N and KH.

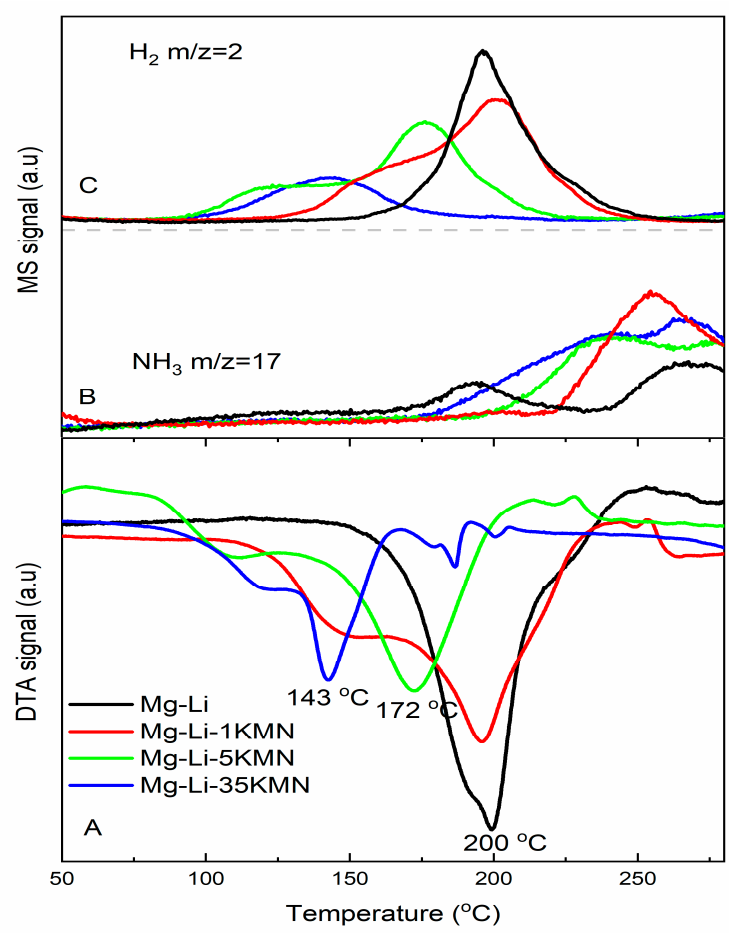

Figure 1. (**A**) Differential thermal analysis (DTA), (**B–C**) Mass spectroscopy (MS) traces of as-milled samples. Heating was applied from room temperature until 300 °C with 3 °C/min heating rate under 50 mL/min Ar flow.

Rietvelt refinement performed on the diffraction patterns acquired after the first dehydrogenation/rehydrogenation cycle (Figure S2) reveals that the specimen is composed of $Mg(NH_2)_2$ (60.6 wt.%), LiH (29.8 wt.%), KH (3.1 wt.%), MgO (3.5 wt.%), and Mn_4N (3 wt.%). Since $K_2Mn(NH_2)_4$ was not present in the in-situ SR-PXD data (Figure 2), we expect that it decomposes into KH and Mn_4N with NH_3 and H_2 release as shown in reaction 2;

$$Mg(NH_2)_2 + 2LiH + K_2Mn(NH_2)_4 \rightarrow Li_2Mg(NH)_2 + 2KH + \frac{1}{4}Mn_4N + xNH_3(g) + yH_2(g) \quad (3)$$

In the literature, some metal nitrides (TaN and TiN) are known to catalytically enhance dehydrogenation of the $2LiNH_2 + MgH_2$ system [20]. Besides that, the Mn_4N + LiH system is known to be an effective catalyst for NH_3 synthesis [46]. Therefore, we firstly studied the possible effect of Mn_4N on the reaction kinetics and thermal behavior of the $Mg(NH_2)_2$ + 2LiH system. However, we could not observe any beneficial effect from Mn_4N either in DSC analysis or in the volumetric H_2 release curves (Figures S3 and S4). Secondly, we investigated the effect of pure KH additions, which is also known to be an effective additive to reduce dehydrogenation peak temperature and improve reaction kinetics of the $Mg(NH_2)_2$ + 2LiH system [21,27]. In order to investigate the effect of KH on the hydrogen sorption properties, three additional samples were prepared with increasing the amount of KH (Mg–Li–7KH, Mg–Li–15KH and Mg–Li–30KH). These samples were prepared at the same milling conditions as Mg–Li–5KMN. Volumetric H_2 release curves of the first dehydrogenation of the prepared samples are presented in Figure 3A. Upon dehydrogenation, Mg–Li shows a release of hydrogen

equal to 4.1 wt.%. The same amount was released in the Mg–Li, Mg–Li–7KH systems. The sample Mg–Li–5KMN has slightly lower H_2 capacity (3.8 wt.%). The amount of released hydrogen decreases to 3.5 wt.% and 3.2 wt.% for the samples Mg–Li–15KH and Mg–Li–30KH, respectively. In order to compare the kinetic behavior of all investigated samples, the measured H_2 capacity was normalized (Figure S5). Apparently, the kinetic behaviors of all additive-containing samples are very similar and they are comparably faster than the pristine Mg–Li. The slow dehydrogenation kinetics obtained from the Mg–Li sample at 180 °C is not surprising, since the corresponding peak temperature observed in the DSC analysis measured under 1 bar of H_2 is as high as 216 °C (Figure 1A).

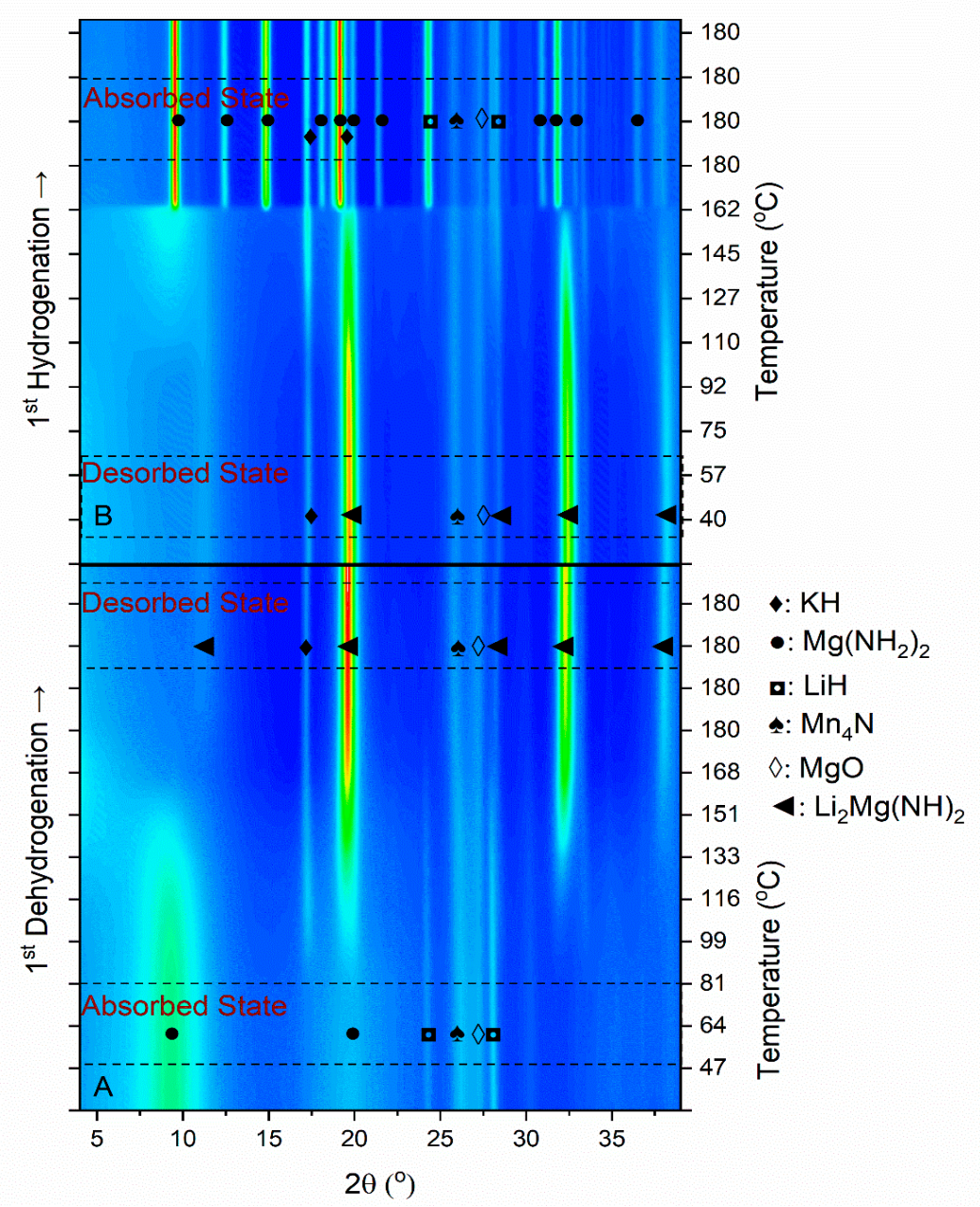

Figure 2. (**A**) In-situ synchrotron powder X-ray diffraction (SR-PXD) pattern for the first dehydrogenation of Mg–Li–5KMN under 1 bar of H_2. (**B**) In-situ SR-PXD pattern for the first hydrogenation of Mg–Li–5KMN under 80 bar of H_2. Sample was heated from RT until 180 °C with 3 °C/min heating rate and each 15 seconds, a SR-PXD data was collected (λ = 0.9941 Å). Additionally, dehydrogenation and hydrogenation experiments were extended to 30 min in isothermal conditions (180 °C).

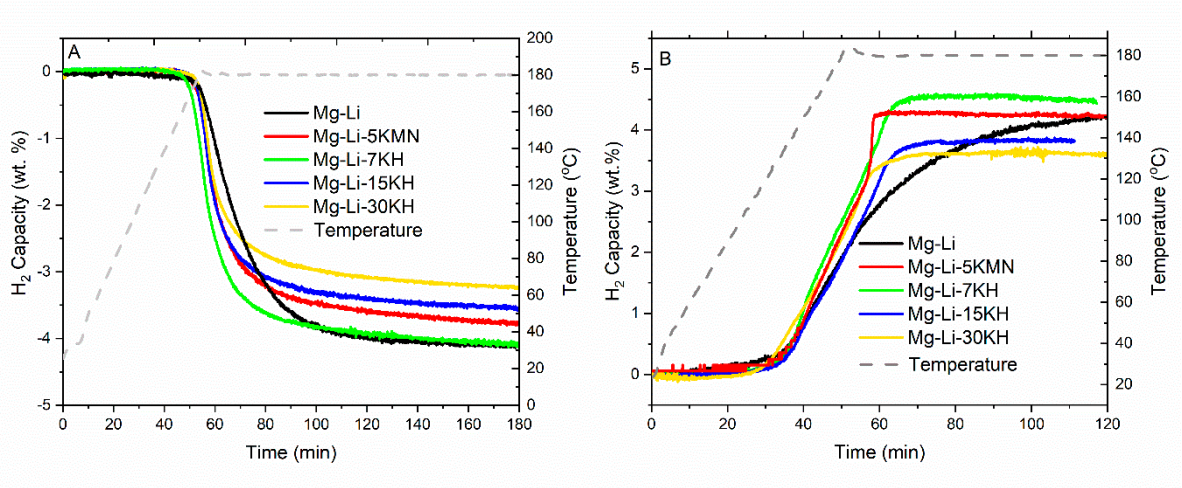

Figure 3. Non-isothermal (**A**) dehydrogenation, (**B**) rehydrogenation kinetics of prepared samples. Heating was applied from room temperature until 180 °C, with a heating rate of 3 °C/min. Dehydrogenation and rehydrogenation were carried out under 1 bar and 80 bar of H_2, respectively.

The measured rehydrogenation kinetics of all the investigated samples are presented in Figure 3B. The rehydrogenation kinetics of Mg–Li are slower than those of KH-containing samples and those containing $K_2Mn(NH_2)_4$. Interestingly, the rehydrogenation rate of Mg–Li–5KMN noticeably increases toward the end of the hydrogenation. In fact, the last 1 wt.% of H_2 is loaded in only 2 min. This rehydrogenation rate (at this stage of hydrogenation) is four times faster than that of Mg–Li–7KH. This result suggests that the presence of $K_2Mn(NH_2)_4$ and the in-situ dual formation of KH and Mn_4N accelerated the diffusive processes commonly found in the last stage of hydrogenation processes owing to the formation of low H_2 diffusion coefficients of the hydride phases [44].

3.2. Dehydrogenation/Rehydrogenation Properties upon Cycling

This particular feature (rehydrogenation rate increases toward the end of the reaction) is preserved upon the following two dehydrogenation/rehydrogenation cycles (Figure 4). Interestingly, the first hydrogenation is faster than the second, which was observed before with a similar system [36]. Usually, hydrogenation of materials are slower at the later stage [47,48]. In practical applications, fast kinetics are favored [49,50]. In the case of $K_2Mn(NH_2)_4$-containing samples, the fast hydrogenation kinetics at later reaction stages represent an advantage over other hydrogen storage systems, with which full saturation is hardly reached.

The volumetric measurements of the H_2 dehydrogenation for the 1st and 25th cycles of Mg–Li and Mg–Li–5KMN are presented in Figure 5A. Mg–Li–5KMN sample releases 3.8 wt.% of H_2 within 3 hours in the first dehydrogenation. The amount of released H_2 reaches 4.2 wt.% in the second dehydrogenation, due to a longer measurement time. For this system, no noticeable loss in H_2 capacity was observed for 25 cycles. In contrast, the amount of released H_2 for Mg–Li after 25 cycles decreased from 4.2 wt.% to 2.2 wt.%. It is clear that repeated dehydrogenation/rehydrogenation cycles lead to slower reaction kinetics for both samples. It was already reported that for the amide-hydride systems, high operating temperatures cause the agglomeration of dehydrogenation/rehydrogenation products and segregation of reactants and K-based additives [51]. Although reaction kinetics of Mg–Li–5KMN slow down upon cycling, the positive effect of the presence of additives on the reversibility of the sample maintains within the measured 25 cycles. In-situ SR-PXD contour plot of the Mg–Li–5KMN sample at the 25th dehydrogenation (Figure 5B) reveals that identified phases are the same as in the first dehydrogenation (Figure 2A). Thus, once formed, KH and Mn_4N additives remain stable.

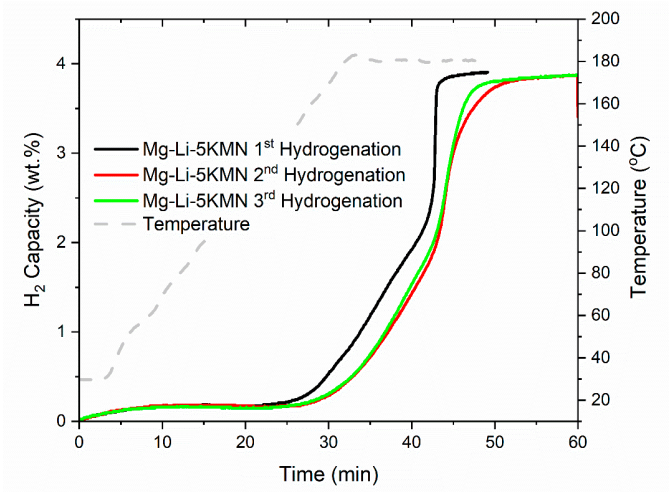

Figure 4. Hydrogenation kinetics of Mg–Li–5KMN for the first three cycles. Sample was heated from room temperature until 180 °C with a heating rate of 5 °C/min under 80 bar of H_2.

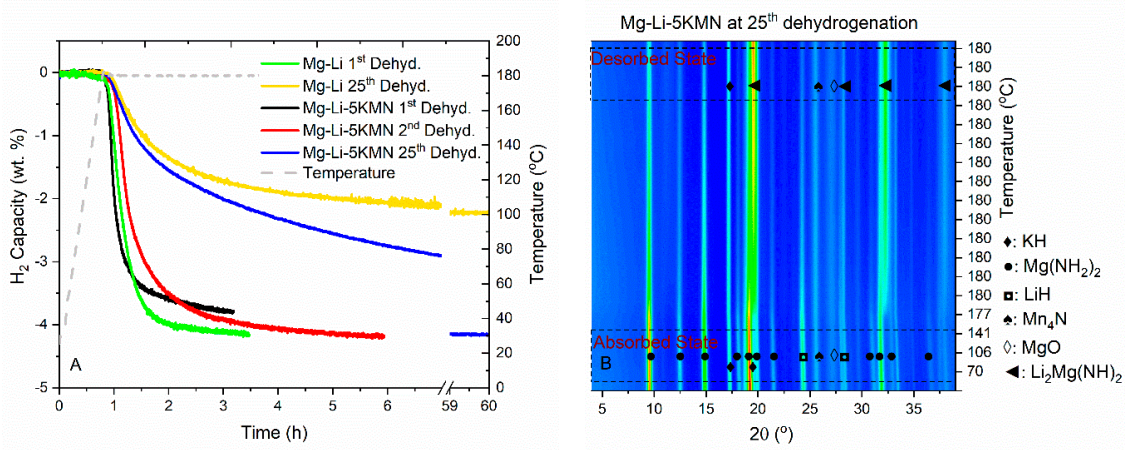

Figure 5. (**A**) Dehydrogenation kinetics of Mg–Li and Mg–Li–5KMN samples in the 1st and 25th cycles. Samples were heated from RT until 180 °C with a heating rate of 5 °C/min under 1 bar of H_2. (**B**) In-situ SR-PXD contour plot of Mg–Li–5KMN at 25th dehydrogenation under 1 bar of H_2. Sample was heated from room temperature until 180 °C with 3 °C/min heating rate, and each 15 seconds, a SR-PXD data was collected (λ= 0.9941 Å). Additionally, dehydrogenation experiment was extended to 120 min at isothermal conditions (180 °C).

3.3. Apparent Activation Energies and Rate Constants

The Kissinger method was applied to calculate the apparent activation energies (E_a) and frequency factor (A) from DSC curves for Mg–Li and Mg–Li–5KMN samples (Figure 6A). Considering the complexity of the reaction, mainly for the material with the additive, the temperatures at the observed maximum reaction rate were taken for the calculation of these parameters (Figures S6 and S7). It is worthy to remind that the dehydrogenation peak temperature of Mg–Li–5KMN was 30 °C lower than that of the pristine Mg–Li (Figure 1A), and reaction kinetics were comparably faster (Figure 3). However, the E_a as well as A values are higher for the Mg–Li–5KMN than for Mg–Li, i.e., 196 ± 5 kJ/mol H_2 and 2.7 × 10^{22}, 161 ± 5 kJ/mol H_2 and 3.5 × 10^{17}, respectively. It is reported that the reaction pathway of KH-added $Mg(NH_2)_2$+2LiH is different under argon and hydrogen atmosphere [27,52]. Dehydrogenation under hydrogen instead of argon alters the dehydrogenation products, which results in an increase of E_a in the case of Mg–Li–5KMN with respect to Mg–Li. This behavior is different from the reports in the literatures, where E_a is lowered with the addition of K-compounds [34,53].

In order to understand these contradictory findings, rate constants (k) were calculated (Figure 6B, Table S1) by the Arrhenius expression $k = A \cdot \exp[-E_a/RT]$ (1/s) at the cycling temperature of 180 °C. Then, k was multiplied with the H_2 capacities obtained from Figure 3A in order to obtain reaction rates (Figure 6B). Despite the fact that Mg–Li–5KMN has a higher E_a value in respect to Mg–Li, the calculated kinetic constant (Table S1) and reaction rate indicate faster kinetic behavior for Li–5KMN at 180 °C. These outcomes are in agreement with the observed kinetic behavior (Figure 3). It suggests that the notable increase of the frequency factor for Mg–Li–5KMN prompts a more efficient interaction between reactants at the interphases, resulting in faster kinetic behavior.

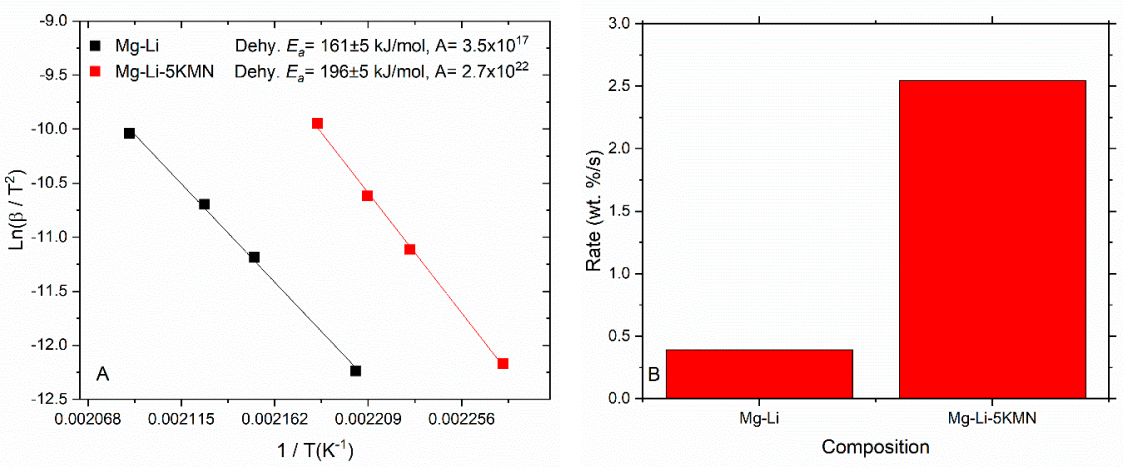

Figure 6. (**A**) Kissinger plots of samples Mg–Li and Mg–Li–5KMN, derived from Differential scanning calorimetry (DSC) curves of the first dehydrogenation reaction at different heating rates (1, 3, 5 and 10 °C/min). Fitting goodness (R^2): 0.9979 for Mg–Li and 0.9985 for Mg–Li–5KMN. (**B**) Calculated reaction rate related to the corresponding samples.

4. Conclusions

The influence of bimetallic amide $K_2Mn(NH_2)_4$ additive on dehydrogenation/rehydrogenation properties of $Mg(NH_2)_2$ + 2LiH system was investigated. In-situ SR-PXD analysis of the as-milled Mg–Li–5KMN reveals that $K_2Mn(NH_2)_4$ decomposes into Mn_4N and a potassium compound with amorphous or nanocrystalline nature. KH appears through the first dehydrogenation. Once formed, Mn_4N and KH remain stable for 25 cycles. The observed dehydrogenation peak temperature of Mg–Li–5KMN is ~30 °C lower than that of Mg–Li. Furthermore, Mg–Li–5KMN has a high storage capacity of 4.2 wt.% of H_2, which is stable for at least 25 cycles. Another positive feature observed in this study is the surprisingly fast rehydrogenation rate at the last stage of the rehydrogenation reaction. Under the applied conditions, hydrogenation of the last 1 wt.% takes place in only 2 min, which is four times faster than in the respective Mg–Li–7KH sample. These fast reaction rates are preserved in the following three cycles. Further investigations should be made to understand this fast reaction behavior and the nature of the dual in-situ-formed additives.

Supplementary Materials: The following are available online at http://www.mdpi.com/1996-1073/12/14/2779/s1, Figure S1: PXD pattern of K and Mn after ball milling under NH_3. λ=Cu, K_α. Based on Rietveld refinement, weight fraction of $K_2Mn(NH_2)_4$: 95 wt.%, $MnH_{0.07}$: 5 wt.%, Figure S2: SR-PXD pattern of the Mg–Li–5KMN after rehydrogenation, λ= 0.9941 Å. Blue dots: Measurement data, Black line: Calculated fit, Figure S3: DSC curves of Mg–Li and 5 mol% Mn_4N containing Mg–Li samples. Heating rate: 3 K/min, Figure S4: H_2 release curves of Mg–Li and 5 mol% Mn_4N containing Mg–Li samples under 1 bar of H_2. Heating: RT → 180 °C, 3 °C/min, Figure S5: Non-isothermal normalized dehydrogenation kinetics of prepared samples. Heating was applied from room temperature until 180 °C, with a heating rate of 3 °C/min. Dehydrogenation was carried out under 1 bar of H_2, Figure S6: DSC and corresponding Arrhenius plots of Mg–Li at the 1st dehydrogenation, Figure S7: DSC and corresponding Arrhenius plots of Mg–Li–5KMN at the 1st dehydrogenation, Table S1: Calculation of the kinetic constant applying the Arrhenius equation.

Author Contributions: Conceptualization, G.G. and H.C.; formal analysis, G.G., J.P. and A.S.; investigation, G.G.; resources, W.Z., T.H. and P.C.; writing—original draft preparation, G.G.; writing—review and editing, C.P., J.P., M.D. and T.K.; supervision, C.P.

Funding: This work was funded by the CAS-HZG collaborative project "RevHy" – "Study on the synthesis, structures and performances of complex hydrides systems for Reversible high capacity Hydrogen storage at low temperatures" H.J., Cao acknowledges the support from the National Natural Science Foundation of China (51801197). The authors thank CONICET (Consejo Nacional de Invetigaciones Científicas y Técnicas) and Alexander von Humboldt Foundation in the frame of the post-doctoral fellowship of J. Puszkiel (Fellowship number: ARG-1187279-GF-P).

Conflicts of Interest: The authors declare no conflict of interest.

References

1. Saldan, I. A prospect for $LiBH_4$ as on-board hydrogen storage. *Cent. Eur. J. Chem.* **2011**, *9*, 761–775. [CrossRef]
2. Klebanoff, L.E.; Keller, J.O. 5 Years of hydrogen storage research in the U.S. DOE Metal Hydride Center of Excellence (MHCoE). *Int. J. Hydrogen Energy* **2013**, *38*, 4533–4576. [CrossRef]
3. Hirscher, M. *Handbook of Hydrogen Storage*; Wiley-VCH Verlag GmbH & Co. KGaA: Weinheim, Germany, 2010.
4. Varin, R.A.; Czujko, T.; Wronski, Z. *Nanomaterials for Solid State Hydrogen Storage*; Springer Publishing Company: New York, NY, USA, 2009.
5. Eberle, U.; Felderhoff, M.; Schüth, F. Chemische und physikalische Lösungen für die Speicherung von Wasserstoff. *Angew. Chemie* **2009**, *121*, 6732–6757. [CrossRef]
6. von Colbe, J.M.B.; Lozano, G.; Metz, O.; Buecherl, T.; Bormann, R.; Klassen, T.; Dornheim, M. Design, sorption behaviour and energy management in a sodium alanate-based lightweight hydrogen storage tank. *Int. J. Hydrogen Energy* **2015**, *40*, 2984–2988. [CrossRef]
7. Orimo, S.; Nakamori, Y.; Eliseo, J.R.; Züttle, A.; Jensen, C.; Complex, M. Hydrides for Hydrogen Storage. *Chem. Rev.* **2007**, *107*, 4111–4132. [CrossRef]
8. Wang, J.; Li, H.W.; Chen, P. Amides and borohydrides for high-capacity solid-state hydrogen storage-Materials design and kinetic improvements. *Mater. Res. Soc.* **2013**, *38*, 480–487. [CrossRef]
9. Chen, P.; Xiong, Z.; Luo, J.; Lin, J.; Tan, K.L. Interaction of hydrogen with metal nitrides and imides. *Nature* **2002**, *420*, 302–304. [CrossRef]
10. Milanese, C.; Jensen, T.R.; Hauback, B.C.; Pistidda, C.; Dornheim, M.; Yang, H.; de Jongh, P.E. Complex hydrides for energy storage. *Int. J. Hydrogen Energy* **2019**, *44*, 7860–7874. [CrossRef]
11. Garroni, S.; Santoru, A.; Cao, H.; Dornheim, M.; Klassen, T.; Milanese, C.; Pistidda, C. Recent progress and new perspectives on metal amide and imide systems for solid-state hydrogen storage. *Energies* **2018**, *11*, 1027. [CrossRef]
12. Wang, H.; Cao, H.; Wu, G.; He, T.; Chen, P. The improved hydrogen storage performances of the multi-component composite: $2Mg(NH_2)_2$-3LiH-$LiBH_4$. *Energies* **2015**, *8*, 6898–6909. [CrossRef]
13. Wang, H.; Cao, H.; Pistidda, C.; Garroni, S.; Wu, G.; Klassen, T.; Chen, P. Effects of Stoichiometry on the H_2 -Storage Properties of $Mg(NH_2)_2$–LiH–$LiBH_4$ Tri-Component Systems. *Chem. Asian J.* **2017**, *12*, 1758–1764. [CrossRef] [PubMed]
14. Leng, H.Y.; Ichikawa, T.; Hino, S.; Hanada, N.; Isobe, S.; Fujii, H. Synthesis and decomposition reactions of metal amides in metal-N-H hydrogen storage system. *J. Power Sources* **2006**, *156*, 166–170. [CrossRef]
15. Luo, W.; Sickafoose, S. Thermodynamic and structural characterization of the Mg-Li-N-H hydrogen storage system. *J. Alloys Compd.* **2006**, *407*, 274–281. [CrossRef]
16. Luo, W.; Rönnebro, E. Towards a viable hydrogen storage system for transportation application. *J. Alloys Compd.* **2005**, *404*, 392–395. [CrossRef]
17. Xiong, Z.; Hu, J.; Wu, G.; Chen, P.; Luo, W.; Gross, K.; Wang, J. Thermodynamic and kinetic investigations of the hydrogen storage in the Li-Mg-N.-H. system. *J. Alloys Compd.* **2005**, *398*, 235–239. [CrossRef]
18. Wang, J.; Li, H.; Wang, S.; Liu, X.; Li, Y.; Jiang, L. The desorption kinetics of the $Mg(NH_2)_2$ + LiH mixture. *Int. J. Hydrogen Energy* **2009**, *34*, 1411–1416. [CrossRef]
19. Li, C.; Liu, Y.; Ma, R.; Zhang, X.; Li, Y.; Gao, M.; Pan, H. Superior dehydrogenation/hydrogenation kinetics and long-term cycling performance of K and Rb Cocatalyzed $Mg(NH_2)_2$-2LiH system. *ACS Appl. Mater. Interfaces* **2014**, *6*, 17024–17033. [CrossRef] [PubMed]

20. Ma, L.P.; Wang, P.; Dai, H.B.; Cheng, H.M. Catalytically enhanced dehydrogenation of Li-Mg-N-H hydrogen storage material by transition metal nitrides. *J. Alloys Compd.* **2009**, *468*, L21–L24. [CrossRef]
21. Wang, J.; Liu, T.; Wu, G.; Li, W.; Liu, Y.; Araújo, C.M.; Yang, P. Potassium-modified $Mg(NH_2)_2$/2LiH system for hydrogen storage. *Angew. Chemie Int. Ed.* **2009**, *48*, 5828–5832. [CrossRef]
22. Amica, G.; Larochette, P.A.; Gennari, F.C. Hydrogen storage properties of $LiNH_2$ –LiH system with MgH_2, CaH_2 and TiH_2 added. *Int. J. Hydrogen Energy* **2015**, *40*, 9335–9346. [CrossRef]
23. Zhao, W.; Jiang, L.; Yuanfang, W.U.; Jianhua, Y.E.; Yuan, B.; Zhinian, L.I.; Shumao, W. Improved dehydrogenation cycle performance of the $1.1MgH_2$-$2LiNH_2$-$0.1LiBH_4$ system by addition of $LaNi_{4.5}Mn_{0.5}$ alloy. *J. Rare Earths* **2015**, *33*, 783–790.
24. Dong, B.X.; Ge, J.; Teng, Y.L.; Gao, J.J.; Song, L. Improved dehydrogenation properties of the $LiNH_2$ –LiH system by doping with alkali metal hydroxide. *J. Mater. Chem. A* **2015**, *3*, 905–911. [CrossRef]
25. Torre, F.; Valentoni, A.; Milanese, C.; Pistidda, C.; Marini, A.; Dornheim, M.; Garroni, S. Kinetic improvement on the CaH_2-catalyzed $Mg(NH_2)_2$ + 2LiH system. *J. Alloys Compd.* **2015**, *645*, S284–S287. [CrossRef]
26. Liang, C.; Liu, Y.; Gao, M.; Pan, H. Understanding the role of K in the significantly improved hydrogen storage properties of a KOH-doped Li-Mg-N.-H. system. *J. Mater. Chem. A* **2013**, *1*, 5031–5036. [CrossRef]
27. Wang, J.; Chen, P.; Pan, H.; Xiong, Z.; Gao, M.; Wu, G.; Wang, J. Solid-solid heterogeneous catalysis: The role of potassium in promoting the dehydrogenation of the $Mg(NH_2)_2$/2LiH composite. *ChemSusChem* **2013**, *6*, 2181–2189. [CrossRef] [PubMed]
28. Zhang, Y.; Xiong, Z.; Cao, H.; Wu, G.; Chen, P. The enhanced hydrogen storage performance of (Mg-B-N-H)-doped $Mg(NH_2)_2$-2LiH system. *Int. J. Hydrogen Energy* **2014**, *39*, 1710–1718. [CrossRef]
29. Shahi, R.R.; Yadav, T.P.; Shaz, M.A.; Srivastva, O.N. Studies on dehydrogenation characteristic of $Mg(NH_2)_2$/LiH mixture admixed with vanadium and vanadium based catalysts (V, V2O5 and VCl3). *Int. J. Hydrogen Energy* **2010**, *35*, 238–246. [CrossRef]
30. Barison, S.; Agresti, F.; Russo, S.L.; Maddalena, A.; Palade, P.; Principi, G.; Torzo, G. A study of the $LiNH_2$-MgH_2 system for solid state hydrogen storage. *J. Alloys Compd.* **2008**, *459*, 343–347. [CrossRef]
31. Luo, W.; Wang, J.; Stewart, K.; Clift, M.; Gross, K. Li-Mg-N-H: Recent investigations and development. *J. Alloys Compd.* **2007**, 336–341. [CrossRef]
32. Li, C.; Liu, Y.; Pang, Y.; Gu, Y.; Gao, M.; Pan, H. Compositional effects on the hydrogen storage properties of $Mg(NH_2)_2$-2LiH-xKH and the activity of KH during dehydrogenation reactions. *Dalt. Trans.* **2014**, *43*, 2369–2377. [CrossRef]
33. Durojaiye, T.; Hayes, J.; Goudy, A. Rubidium hydride: An exceptional dehydrogenation catalyst for the lithium amide/magnesium hydride system. *J. Phys. Chem. C* **2013**, *13*, 6554–6560. [CrossRef]
34. Durojaiye, T.; Hayes, J.; Goudy, A. Potassium, rubidium and cesium hydrides as dehydrogenation catalysts for the lithium amide/magnesium hydride system. *Int. J. Hydrogen Energy* **2015**, *40*, 2266–2273. [CrossRef]
35. Cao, H.; Santoru, A.; Pistidda, C.; Richter, T.M.; Chaudhary, A.L.; Gizer, G.; Dornheim, M. New synthesis route for ternary transition metal amides as well as ultrafast amide-hydride hydrogen storage materials. *Chem. Commun.* **2016**, *52*, 5100–5103.
36. Cao, H.; Richter, T.M.M.; Pistidda, C.; Chaudhary, A. Ternary Amides containing transition metals for hydrogen storage: A Case study with alkali metal amidozincates. *ChemSusChem* **2015**, *8*, 3777–3782. [CrossRef] [PubMed]
37. Cao, H.; Pistidda, C.; Richter, T.M.; Santoru, A.; Milanese, C.; Garroni, S.; Niewa, R. In situ x-ray diffraction studies on the de/rehydrogenation processes of the $K_2[Zn(NH_2)_4]$-8LiH system. *J. Phys. Chem. C* **2017**, *121*, 1546–1551. [CrossRef]
38. Cerenius, Y.; Ståhl, K.; Svensson, L.A.; Ursby, T.; Oskarsson, Å; Albertsson, J.; Liljas, A. The crystallography beamline I711 at MAX II. *J. Synchrotron Radiat.* **2000**, *7*, 203–208. [CrossRef]
39. Rietveld, H.M. A profile refinement method for nuclear and magnetic structures. *J. Appl. Crystallogr.* **1968**, *2*, 65–71. [CrossRef]
40. Lutterotti, L. Total pattern fitting for the combined size-strain-stress-texture determination in thin film diffraction. *Nucl. Instrum. Methods Phys. Res. Sect. B Beam Interact. Mater. Atoms* **2010**, *268*, 334–340. [CrossRef]
41. Bösenberg, U.; Pistidda, C.; Tolkiehn, M.; Busch, N.; Saldan, I.; Suarez-Alcantara, K.; Dornheim, M. Characterization of metal hydrides by in-situ XRD. *Int. J. Hydrogen Energy* **2014**, *39*, 9899–9903. [CrossRef]

42. Pistidda, C.; Santoru, A.; Garroni, S.; Bergemann, N.; Rzeszutek, A.; Horstmann, C.; Dornheim, M. First direct study of the ammonolysis reaction in the most common alkaline and alkaline earth metal hydrides by in situ SR-PXD. *J. Phys. Chem. C* **2015**, *119*, 934–943. [CrossRef]
43. Hammersley, A.P. *FIT2D: AN Introduction and Overview*; ESRF internal report ESRF97HA02T; European Synchrotron Radiation Facility (ESRF): Grenoble, France, 1997; Available online: http://www.esrf.eu/computing/scientific/FIT2D/FIT2D_INTRO/fit2d.html (accessed on 1 May 2019).
44. Kissinger, H.E. Reaction kinetics in differential thermal analysis. *Anal. Chem.* **1957**, *29*, 1702–1706. [CrossRef]
45. Hu, J.; Liu, Y.; Wu, G.; Xiong, Z.; Chen, P. Structural and compositional changes during hydrogenation/dehydrogenation of the Li-Mg-N.-H. system. *J. Phys. Chem. C* **2007**, *111*, 18439–18443. [CrossRef]
46. Wang, P.; Chang, F.; Gao, W.; Guo, J.; Wu, G.; He, T.; Chen, P. Breaking scaling relations to achieve low-temperature ammonia synthesis through LiH-mediated nitrogen transfer and hydrogenation. *Nat. Chem.* **2017**, *9*, 64–70. [CrossRef] [PubMed]
47. Dornheim, M. Thermodynamics of Metal Hydrides: Tailoring Reaction Enthalpies of Hydrogen Storage Materials. In *Thermodynamics-Interaction Studies-Solids, Liquids and Gases*; InTech: Rijeka, Croatia, 2012; pp. 892–918.
48. Bogdanovic, B.; Ritter, A.; Spliethoff, B. Active MgH_2-Mg systems for reversible chemical energy storage. *Angew. Chem.* **1990**, *29*, 223–328. [CrossRef]
49. Capurso, G.; Schiavo, B.; Jepsen, J.; Lozano, G.A.; Metz, O.; Klassen, T.; Dornheim, M. Metal hydride-based hydrogen storage tank coupled with an urban concept fuel cell vehicle: Off board tests. *Adv. Sustain. Syst.* **2018**, *2*, 1800004. [CrossRef]
50. Baricco, M.; Bang, M.; Fichtner, M.; Hauback, B.; Linder, M.; Luetto, C.; Sgroi, M. SSH2S: Hydrogen storage in complex hydrides for an auxiliary power unit based on high temperature proton exchange membrane fuel cells. *J. Power Source* **2017**, *342*, 853–860. [CrossRef]
51. Li, C.; Liu, Y.; Yang, Y.; Gao, M.; Pan, H. High-temperature failure behaviour and mechanism of K-based additives in Li-Mg-N-H hydrogen storage systems. *J. Mater. Chem. A* **2014**, *2*, 7345–7353. [CrossRef]
52. Liu, Y.; Yang, Y.; Zhang, X.; Li, Y.; Gao, M.; Pan, H. Insights into the dehydrogenation reaction process of a K-containing $Mg(NH_2)_2$-2LiH system. *Dalt. Trans.* **2015**, *44*, 18012–18018. [CrossRef]
53. Liu, Y.; Li, C.; Li, B.; Gao, M.; Pan, H. Metathesis reaction-induced significant improvement in hydrogen storage properties of the KF-added $Mg(NH_2)_2$-2LiH system. *J. Phys. Chem. C* **2013**, *117*, 866–875. [CrossRef]